# Characteristics of Tornado-Like Vortices Simulated in a Large-Scale Ward-Type Simulator

**Zhuo Tang • Changda Feng • Liang Wu • Delong Zuo • Darryl L. James**

Received: DD Month YEAR/ Accepted: DD Month YEAR

**Abstract** Tornado-like vortices are simulated in a large-scale Ward-type simulator to further advance the understanding of such flows, and to facilitate future studies of tornado wind loading on structures. Measurements of the velocity fields near the simulator floor and the resulting floor surface pressures are interpreted to reveal the mean and fluctuating characteristics of the flow as well as the characteristics of the static-pressure deficit. We focus on the manner in which the swirl ratio and the radial Reynolds number affect these characteristics. The transition of the tornado-like flow from a single-celled vortex to a dual-celled vortex with increasing swirl ratio and the impact of this transition on the flow field and the surface-pressure deficit are closely examined. The mean characteristics of the surface-pressure deficit caused by tornado-like vortices simulated at a number of swirl ratios compare well with the corresponding characteristics recorded during full-scale tornadoes.

**Keywords** Aspect ratio • Radial Reynolds number • Surface-pressure deficit • Swirl ratio • Tornado-like vortex

## 1 Introduction

Tornadoes are historically among the most devastating natural hazards resulting from the flow in the atmospheric boundary layer. Even given today's advances in science and technology, especially the significant improvement in building practice, the devastation caused by tornadoes

Delong Zuo • Zhuo Tang • Changda Feng • Liang Wu
Department of Civil, Environmental and Construction Engineering, Texas Tech University, Lubbock, TX 79409, USA.
e-mail: delong.zuo@ttu.edu

Darryl L. James
Department of Mechanical Engineering, Texas Tech University, Lubbock, TX 79409, USA.

has not subsided. Indeed, several recent major tornadoes in the U.S.A., including the Joplin (Missouri) and Tuscaloosa–Birmingham (Alabama) tornadoes in 2011, the Moore (Oklahoma) tornado in 2013 and the Dallas (Texas) area tornado in 2015, have each caused more than one billion US dollars in monetary losses and tens of fatalities, and in the case of the Joplin tornado, more than 100 fatalities.

A major reason for the continued devastation resulting from tornadoes is the inadequate understanding of their loading on structures. Due to the destructive nature of tornadoes and the difficulty in predicting their formation and subsequent path, the measurement of full-scale wind speeds in tornadoes remains challenging. The existing measurements have mostly been recorded with Doppler radars (e.g., Wurman and Alexander 2005), and the measurements of tornado-generated pressure deficits have only been made by probes on the ground (e.g., Karstens et al. 2010) in a limited number of cases. While Doppler radar measurements have been extensively used in studies of the genesis and large-scale characteristics of tornadoes, the resolution of these measurements is inadequate for the investigation of turbulence in tornadoes or the resulting wind loading on structures. Also, since radars must be stationed at long distances from tornadoes, the measurements can only be made above the heights of many structures, such as low-rise buildings, which are among the most susceptible to damage. For these reasons, many studies have been based on laboratory or numerical simulations. Numerical simulation of tornadic winds, such as those based on computational fluid dynamics, has particularly undergone steady progress in recent years (e.g., Lewellen et al. 1997, Nolan and Farrell 1999, Nolan 2005, Ishihara et al. 2011, Natarajan and Hangan 2012). However, the capability of this approach in assessing the turbulence in tornadoes still needs to be validated using either full-scale or laboratory data.

The laboratory simulation of tornado-like flows has seen significant advancements since Ying and Chang (1970) built the first tornado simulator more than four decades ago. In particular, the so-called Ward-type simulator, which is named after its inventor (Ward 1972), has undergone continued development. This type of simulator utilizes a fan or multiple fans at the top to generate an updraft, and a mechanism at the periphery of the cylindrical testing chamber at the bottom to control the angular momentum of the inflow. A baffle between the convective region above the updraft hole and a plenum below the exhaust eliminate the influence of the vorticity created by the fan(s) on the flow below the baffle. Initially, a rotating screen, first without (Ward 1972) and then with (Church et al. 1977) surrounding anti-turbulence panels, was used to control the circulation in the inflow. More recent designs have opted to use turning vanes in the form of airfoils for this purpose (e.g., Lund and Snow 1993, Mishra et al. 2008).

Experiments in Ward-type simulators have historically contributed to the fundamental understanding of tornado-like flows, as well as the dependence of the flow structure on the swirl ratio, the radial Reynolds number, and the aspect ratios, which have been identified to be the non-dimensional parameters governing the dynamics and geometry of three-dimensional vortex flows (Lewellen 1962, Davies-Jones 1973). Based on the qualitative interpretation of flow visualization and quantitative analysis of the velocity and surface-pressure measurements, previous investigations (e.g., Ward 1972, Davies-Jones 1973, Jischke and Parang 1974, Church et al. 1979, Snow et al. 1980, Lund and Snow 1993) suggested that the swirl ratio is the primary parameter controlling the structure of simulated vortices. A single-celled vortex forms at a small swirl ratio, and with increasing swirl ratio, the core of the vortex transitions from a laminar to a turbulent state. The transition initiates from a region near the flow-straightening baffle and continues to progress upstream until reaching the simulator floor. With a further increase of the swirl ratio, the flow transitions into a dual-celled vortex, resulting in downflow in the region surrounding the axis of the simulator and, ultimately, to multiple vortices. Such a transition of the flow was found to be accompanied by a distinct evolution of characteristics such as the radius of the vortex core and the profiles of the mean tangential, radial and axial velocity components, as well as the corresponding change of the radial profile of the mean surface-pressure deficit (e.g., Church et al. 1979, Snow et al. 1980). Compared with the swirl ratio, the radial Reynolds number and aspect ratios were found to only have secondary effects on the simulated flow. In particular, it has been shown that the main characteristics of the mean flow are asymptotically independent of the radial Reynolds number as this number attains sufficiently large values (Church et al. 1979).

While the Ward-type simulator has long been capable of generating flows resembling the main characteristics of natural tornadoes (e.g., Church et al. 1979), most of this type of simulator are small in size and not suitable for applications such as the testing of structural models at adequate geometrical scales (Refan et al. 2014). In addition, because conventional Ward-Type simulators are designed to generate nominally stationary vortices, they cannot be used to study the effects of tornado translation without employing a moving floor. Two types of facilities have been developed in recent years to overcome these two limitations (Haan et al. 2008, Refan and Hangan 2016, Wang et al. 2016). One type is the tornado simulator at Iowa State University, together with a number of similar simulators of the same design. This type of simulator differs from the Ward-type simulators in that it translates and is of a closed-circuit type. The angular momentum is induced by turning vanes at the top of an annular duct above the test section, which contrasts to an open-circuit Ward-type with the angular momentum introduced through a mechanism surrounding the test chamber. The other facility is the Wind Engineering, Energy and Environment Dome at the University of Western Ontario, which, when configured for tornado simulations, is fundamentally similar to that of a Ward-type simulator. However, it uses individually controllable fans at the periphery of the test chamber to supplement the turning vanes and enhance the control of the inflow. It also utilizes a traversing bell mouth to provide a translating source of the updraft to enable the simulation of translating vortices. Both the Iowa State University simulator and a scaled-down model of the facility at the University of Western Ontario have been demonstrated to be capable of simulating tornado-like vortices (Haan et al. 2008, Refan and Hangan 2016).

Regardless of the simulator type, most laboratory simulations of tornadoes to date have been conducted over a smooth surface. In a small number of studies, experiments have been conducted over roughness elements (e.g., Dessens 1972, Zhang and Sarkar 2008, Matsui and Tamura 2009, Wang et al. 2017) representing the roughness of the Earth's surface. These experiments revealed that the surface roughness can substantially affect the mean characteristics of the flow and the surface pressure, such as the size of the vortex core, the magnitude of the mean tangential velocity component and the maximum mean deficit in surface pressure. Although some specific observations have varied from experiment to experiment, the general consensus is that the effects of increasing the surface roughness on the mean flow characteristics is similar to decreasing the swirl ratio (Wang et al. 2017). In a recent study, Wang et al. 2017 observed that the surface roughness affects both the radial and vertical velocity fluctuations. Despite these previous efforts, however, proper configuration of the surface roughness for different types of tornado simulators, or different simulator configurations, remains a challenge due to the inconsistency regarding the geometrical scaling of tornado simulations, and the lack of established criteria for characterizing the surface roughness. Much work is still needed to enable effective quantification of surface-roughness effects on the mean and turbulent structure of tornado-like vortices.

Despite the continued advancement in laboratory simulations of tornado-like vortices, some basic physical characteristics have yet to be comprehensively investigated. In particular, previous studies have primarily focused on the mean components of both the velocity and static-pressure deficit at the surface, with the fluctuating components generally overlooked. In the limited number of experiments performed to study the turbulence, the focus was placed on the root-mean-square values or standard deviations of the tangential, radial and axial velocity components (Tari et al. 2010, Liu and Ishihara 2015, Refan et al. 2015, Wang et al. 2017). While some studies did investigate the Reynolds-stress components and the turbulent kinetic energy (e.g., Tari et al. 2010), lacking are characteristics such as the probability distributions of the velocity and the surface-pressure fluctuations.

A comprehensive experimental campaign was conducted to characterize the mean and fluctuating velocity components of tornado-like vortices simulated in a large-scale Ward-type simulator, with an emphasis on the fluctuations of velocity and surface pressure, which are critical for the tornado loading on structures, as well as the dependence of the turbulence and the surface-pressure fluctuation on the swirl ratio and the radial Reynolds number. Some of the key flow and pressure-deficit characteristics observed in the experiments are compared with the corresponding characteristics of previous important experiments for the understanding of tornadic flows, which enables an assessment of the capability of the simulator to generate tornado-like vortices. All the experiments have been conducted over the smooth floor of the simulator without simulation of tornado translation. Investigations of the effects of surface roughness and tornado translation will be pursued in future experiments after upgrading the facility to enable the simulation of translating tornado-like vortices.

## 2 Experimental Facilities

### 2.1 The tornado simulator

The experiments were conducted in a large-scale Ward-type simulator at Texas Tech University known as the VorTECH simulator. As schematically depicted in Fig. 1, this simulator has a chamber of 10.2 m in diameter, an updraft hole of octagonal cross-section 4 m in diameter, 64 turning vanes in the form of symmetric airfoils at the periphery of the chamber, eight fans at the top, and a honeycomb that functions as the baffle. To generate flows of a desired structure, the orientations of the turning vanes can be varied to control the angular momentum of the inflow, the speed of the fans can be varied to control the amount of updraft, and the heights of the chamber and the turning vanes can be adjusted between 1 m and 2 m to control the internal aspect ratio of the apparatus. A vortex simulated in the VorTECH facility is presented in Fig. 1 as an illustration.

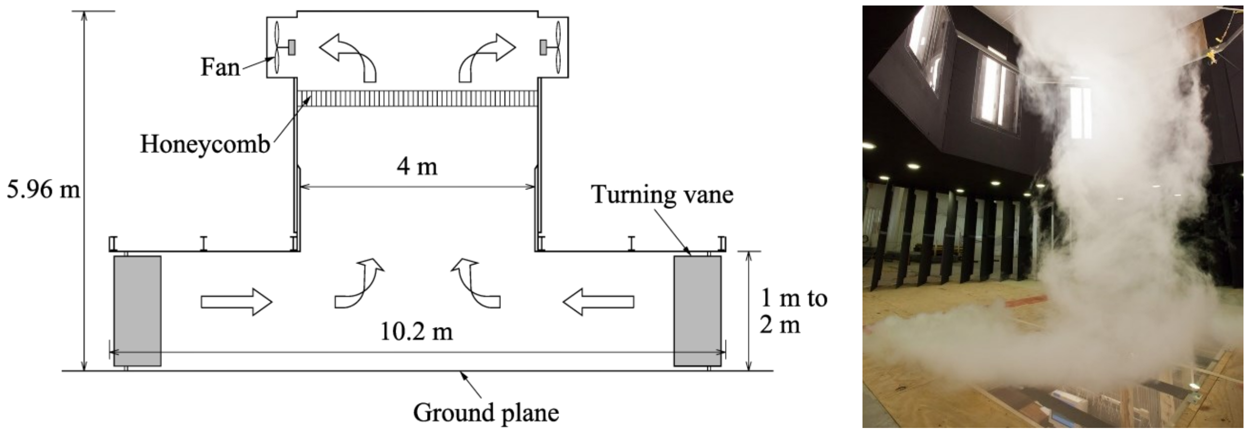


**Fig 1** A Schematic illustration of the VorTECH simulator and a picture of a simulated tornado-like vortex.

## 2.2 Velocity and pressure measurement systems

Measuring the velocity of tornado-like flows in simulators has always been challenging because of the highly three dimensional and turbulent nature of the flow. A 4-hole Cobra probe (Turbulent Flow Instrumentation Pty Ltd) with a dedicated data acquisition system and a 12-hole Omniprobe (Aeroprobe Corporation) sampled by a Scanivalve pressure scanner were used for the velocity measurements, with these probes chosen for their complementing characteristics. When properly configured, the Cobra probe samples at frequencies up to 2000 Hz, but only detects incoming flow within a ±45° cone. By contrast, the Omniprobe detects incoming flow within ±150°, but cannot accurately measure the turbulence. For this reason, the Cobra probe was used for velocity measurements whenever at least 98% of the flow was reported by the manufacturer-supplied software to be within a ±45° cone; otherwise the Omniprobe was used for the measurement of mean velocities.

Probes inserted into the flow are inherently intrusive regardless of the probe type. The Cobra probe has a 0.0026-m head and a maximum stem diameter of 0.014 m, and the Omniprobe has a spherical tip of 0.006-m diameter and a maximum stem diameter of 0.0063 m, which, together with the rods of 0.0125 m diameter for supporting the probes, are not trivial presences in the flow field. However, because the effects of the intrusiveness of the probes on the velocity measurements are compensated by factory-supplied calibrations, the measurements by the probes can be considered acceptable unless the core of the vortex is very small, or the measurement is in regions of very unsteady flow. Indeed, as the experiments show that neither probe provides consistent measurements of the velocities near the vortex axis, velocity measurements in this region are discarded. Further, alternative approaches for velocity measurements in simulated tornado-like vortices, such as those that utilize hotwires or particle image velocimetry, have also been recognized to have their respective limitations (e.g., Church et al. 1979, Refan and Hangan 2016). In this sense, interpretation of the flow field based on measurements by the Cobra probe and the Omniprobe can be considered viable, so long as the limitations of the resultant datasets are recognized.

In addition to the velocity measurements, the static pressures at 195 axisymmetric taps evenly spaced at 0.0191 m along a radial line on the simulator floor (henceforth referred to simply as surface pressures) were also measured in the experiments. The Scanivalve system used to sample the Omniprobe was also used for the pressure measurements.

The reference pressure for the velocity and pressure measurements was chosen as the barometric pressure in a static bottle in the control room beneath the tornado simulator. The static bottle served as a fluid capacitor for attenuating the fluctuation of the barometric pressure. The Cobra probe sampled at 625 Hz to enable recording of the high-frequency flow fluctuations, and the pressure scanners for the Omniprobe and pressure taps sampled at 300 Hz, with each individual velocity and pressure measurement of 2-min duration. For each experimental configuration, velocity measurements were conducted only once, but measurements of the surface pressure were repeated 10 times to provide ensembles and a more accurate estimation of the pressure statistics.

## 3 Estimation of Controlling Parameters

As is now well-recognized, the swirl ratio and the radial Reynolds number control the dynamics of simulated tornado-like vortices and, with the external aspect ratios of tornado simulators often fixed, the internal aspect ratio controls the geometry of the vortices (e.g., Church et al. 1979). The swirl ratio, the radial Reynolds number and the internal aspect ratio (simply the aspect ratio hereafter) are defined in this study as

$$S = r_0 \Gamma / (2Qh), \quad (1)$$

$$Re_r = Q / (2\pi \nu) \quad (2)$$

and

$$a = h / r_0, \quad (3)$$

respectively, where $h$ and $r_0$ are the depth and radius of the convergence region of the flow, which correspond to the height of the turning vanes and the radius of the updraft hole of the VorTECH facility, respectively, $Q$ is the volumetric flow rate per unit axial length, $\Gamma$ is the circulation, and $v$ is the kinematic viscosity.

While the calculation of the aspect ratio is straightforward, the manner in which the swirl ratio and the radial Reynolds number are estimated have varied in previous studies depending on how the volumetric flow rate per unit length and the circulation are estimated. Here, the velocities of the flow at elevations along a vertical line at the edge of the convergence region (i.e., at the radial position $r = r_0$, where $r$ is the horizontal distance from the axis of the chamber) spanning both the simulator floor and the bottom of the updraft hole are used as the basis for the calculation of the volumetric flow rate and the circulation. Assuming that the mean velocity components are axisymmetric, the volumetric flow rate per unit length and the circulation are estimated as

$$Q = 2\pi r_0 \sum_{n=1}^{N} \left( V_{r,n} \times \Delta h_n \right) / h \tag{4}$$

and

$$2\pi r_0 \sum_{n=1}^{N} \left( V_{\theta,n} \times \Delta h_n \right) / h \tag{5}$$

respectively, where $V_{r,n}$ and $V_{\theta,n}$ are the mean radial and tangential velocity components at the $n^{\text{th}}$ measurement point, $\Delta h_n$ is half the distance between the two measurement points surrounding this point, and $N$ is the total number of measurement points.

## 4 Experimental Configurations

As the heights of the chamber and the turning vanes were fixed at 2 m, the aspect ratio of the simulator is, therefore, unity. To investigate the dependence of the simulated flow on the swirl ratio, the angles of the turning vanes were radially varied between 10° and 65°. At each turning vane angle, the speeds of the fans were varied to enable an assessment of the effects of the radial Reynolds number on both the surface-pressure deficit and, for a few turning vane angles, the flow field. Because a major objective of the study is to provide a context for future studies of tornado loading on structures, such as low-rise buildings, the velocity measurements focused on the flow over the lowest quarter of the chamber (i.e., up to 0.5 m above the floor). With the assumption that the mean and turbulent characteristics of the simulated vortices are axisymmetric, all the velocity measurements were recorded within a vertical plane through the axis of the simulator. The distribution of the velocity measurement grid along the vertical direction was the same for all the simulator configurations. Due to the size of the Omniprobe, the lowest elevation of the velocity measurements was 0.01 m above the floor. The vertical resolution of the measurements varied from 0.005 m over the lower elevations to 0.05 m over the higher elevations with some additional intermediate resolutions. The exact vertical resolutions of the velocity measurements are listed in Table 1. The number and locations of the measurement points along the radial direction were varied to ensure an adequate spatial range and resolution of measurements, so that the maximum mean tangential velocity component at every measurement elevation could be approximately captured, and the characteristics of the flow both inside and outside the radial positions of the maximum mean tangential velocity component could be evaluated. The highest horizontal resolution of the measurement was 0.02 m, which was used in regions surrounding the radial positions of the maximum mean tangential velocity component at each measurement elevation.

| Elevation above floor (m) | 0.01 – 0.05 | 0.05 – 0.1 | 0.1 – 0.2 | 0.2 – 0.26 | 0.26 – 0.3 | 0.3 – 0.5 |
|---|---|---|---|---|---|---|
| Measurement resolution (m) | 0.005 | 0.01 | 0.02 | 0.03 | 0.04 | 0.05 |

**Table 1** Vertical resolution of the velocity measurements.

## 5 Characteristics of Simulated Flow and the Resultant Surface-Pressure Deficit

In the following, certain mean and turbulent characteristics of the flow in representative vortices generated for four distinct swirl ratios, as well as the mean and fluctuating characteristics of the corresponding surface-pressure deficit, are interpreted, with the focus on the dependence of these characteristics on the swirl ratio. To facilitate this interpretation, the following conventions and definitions are introduced. The axial and radial velocity components are deemed positive upwards and towards the axis of the simulator, respectively. Considering previous studies observed distinct differences between the flow characteristics inside and outside the radial positions of the maximum mean tangential velocity component, the radial coordinates of these positions and the corresponding mean tangential velocity component are defined to facilitate normalization of the radial coordinates and the velocity components. The local maximum mean tangential velocity component $V_{\theta z\max}$, and the global maximum mean tangential velocity component $V_{\theta\max}$, are defined as the maximum mean tangential velocity component at the elevation $z$ above the floor and the maximum of the local maximum mean tangential velocity component, respectively (i.e., $V_{\theta\max} = \max(V_{\theta z\max})$). Correspondingly, the local core radius $r_{cz}$ and the representative core radius $r_c$ of the simulated vortex are defined as the radial distances between the axis of the simulator and the local maximum mean tangential velocity component at height $z$ and the global maximum mean tangential velocity component, respectively. The height at which the global maximum mean tangential velocity component is achieved is denoted $z_c$.

## 5.1 Mean velocity components

As expected, the structures of the simulated vortices are observed to depend critically on the swirl ratio. Figure 2 shows the mean flow fields of four representative vortices generated at swirl ratios of 0.17, 0.22, 0.36 and 0.84. Flows at these four swirl ratios are selected for a comprehensive characterization, because surface-pressure measurements presented below indicate that the critical transition of the flow from a single-celled vortex to a dual-celled vortex occurs at a swirl ratio of approximately 0.25. In particular, this selection enables a characterization of the flow evolution from a single-celled vortex at a lower swirl ratio to a single-celled vortex immediately before the critical transition, and then from a dual-celled vortex immediately post-transition to a dual-celled vortex at a higher swirl ratio. The radial Reynolds numbers for all four simulations are between $3.11 \times 10^5$ and $4 \times 10^5$. As previous studies have suggested (e.g., Church et al. 1979), the mean characteristics of the simulated flow are essentially independent of the radial Reynolds number over this range. The arrows in the graphs represent the resultant of the mean radial and axial velocity components, with each arrow corresponding to a physical measurement point from either the Cobra probe or Omniprobe. The background colours represent the magnitudes of the mean tangential velocities resulting from a linear interpolation of the measurements.

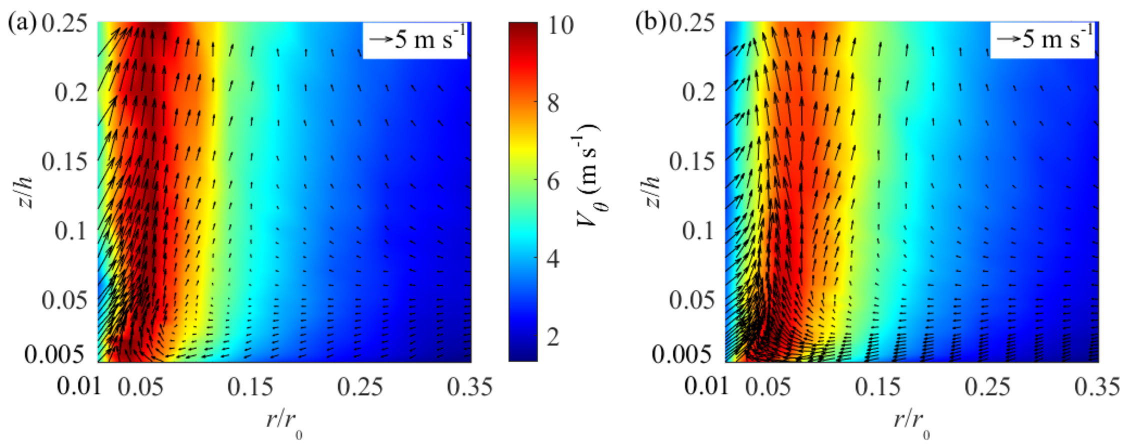

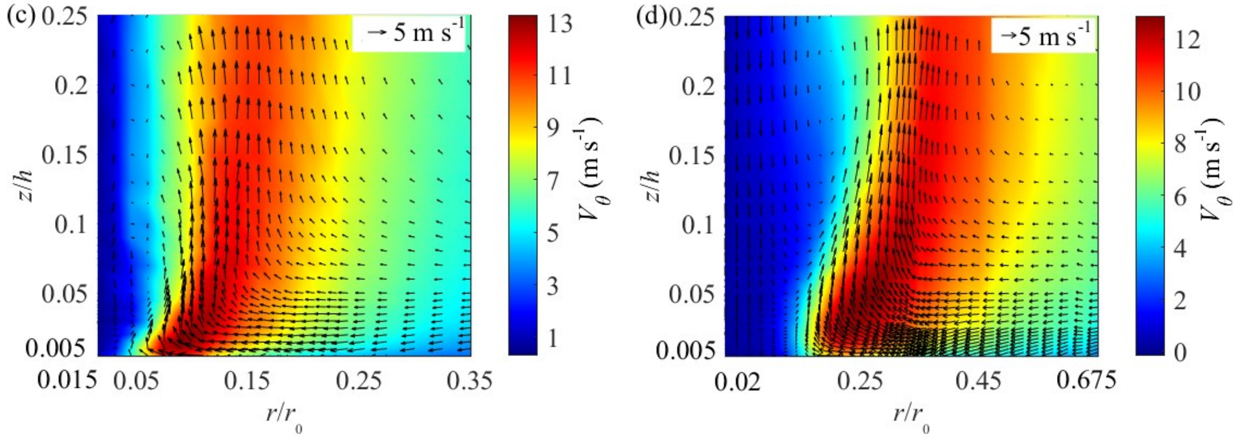


**Fig 2** Mean flow fields at swirl ratios of (a) $S$ = 0.17, (b) $S$ = 0.22, (c) $S$ = 0.36 and (d) $S$ = 0.84.

For the range of swirl ratios considered, the vortices generated at larger swirl ratios have larger cores based on the volume enclosed by the local core radii. Indeed, as shown in Table 2, the representative core radii of the two vortices at the two largest swirl ratios are much larger than those of the two vortices simulated at the two smallest swirl ratios. It also can be seen that the swirl ratio critically affects the structure of the mean radial and axial velocity components. Mostly notably, at swirl ratios of 0.17 and 0.22, the mean axial velocity component is positive at every measurement point inside the cores of the vortices, while, by contrast, an apparent downdraft develops inside the cores of the two vortices simulated at swirl ratios of 0.36 and 0.84, respectively. As suggested by previous studies (e.g., Church et al. 1979, Refan and Hangan 2016), this reflects the evolution of the flow from a single-celled vortex at lower swirl ratios to a dual-celled vortex at higher swirl ratios after vortex breakdown reaches the floor of the simulator at the critical swirl ratio. The evidence shown in Fig. 2, in particular, reveals that the critical swirl ratio separating the single-celled and dual-celled vortex regimes is between 0.22 and 0.36. In addition, Fig. 2 also shows that for the two single-celled vortices, the axial velocity component near the axis is smaller at the larger swirl ratio as caused by the development of an adverse axial pressure gradient resulting from the broadening of the vortex core with increasing swirl ratio (Church et al. 1979). In contrast, for swirl ratios of 0.36 and 0.84, the magnitudes of the downdraft velocities are larger at the higher swirl ratio.

| Swirl ratio ($S$) | Global maximum tangential velocity component ($V_{\theta\max}$) (m s$^{-1}$) | Representative core radius ($r_c$) (m) |
|---|---|---|

| | | |
|---|---|---|
| 0.17 | 10.1 | 0.10 |
| 0.22 | 12.7 | 0.10 |
| 0.36 | 13.3 | 0.18 |
| 0.84 | 12.9 | 0.52 |

**Table 2** Global maximum tangential velocity component and core radius of four tornado-like vortices.

The effects of the swirl ratio on the evolution of the vortex core can also be observed in Fig. 3, which shows the axial profiles of the local core radii and local maximum mean tangential velocity component for the four vortices. According to Fig. 3a, before the transition of the flow from a single-celled vortex to a dual-celled vortex, the broadening of the core moves upstream (i.e., towards the floor) when the swirl ratio increases from 0.17 to 0.22. As previous studies have revealed (Church et al. 1979, Refan and Hangan 2016), this is due to the progression of vortex breakdown from the downstream to upstream direction with increasing swirl ratio over this swirl ratio range. In addition, Fig. 3b shows that, for the lowest swirl ratio of 0.17, the local maximum mean tangential velocity component is almost constant over the height of the measurements. For swirl ratios close to or higher than the value at which the single-celled to dual-celled vortex transition occurs, the local maximum mean tangential velocity component first increases rapidly with height to a maximum value very close to the floor, and then decreases slowly with height thereafter.

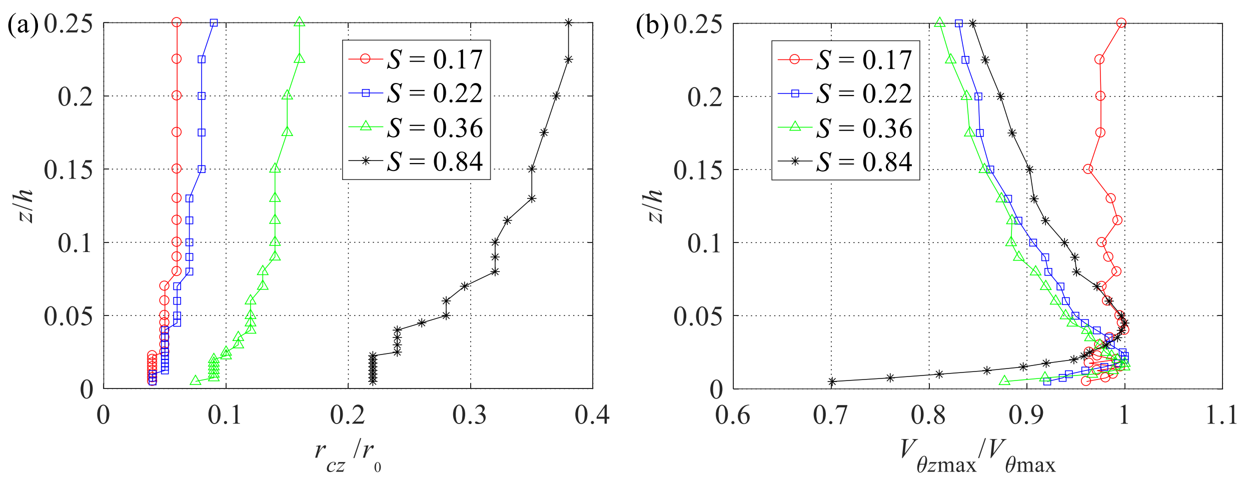


**Fig 3** Profiles of (a) local core radius and (b) maximum mean tangential velocity component at four swirl ratios.

To further investigate the dependence of the mean structure of the simulated vortex on the swirl ratio, the profiles of the mean tangential and radial ($V_r$) velocity components at representative heights and radial positions are examined. Figure 4 shows the radial profiles of the normalized mean tangential velocity component at the height of the maximum mean tangential velocity component $z_c$, and those at two heights below and two heights above $z_c$ for the four vortices. Also included in the graphs are the radial profiles of the mean tangential velocity component according to the modified Rankine combined-vortex model with a decay constant of 0.7, the Burgers-Rott model for single-celled vortices ($S$ = 0.17 and $S$ = 0.22) and the Sullivan model for dual-celled vortices ($S$ = 0.36 and $S$ = 0.84). The radial profile of mean tangential velocity component prescribed by the Rankine combined-vortex model can be expressed as (Wurman et al. 2007)

$$V_\theta = \begin{cases} (r/r_{cz})V_{\theta z\max} & r \le r_{cz} \\ (r_{cz}/r)^{0.7} V_{\theta z\max} & r > r_{cz} \end{cases}, \qquad (6)$$

while that prescribed by the Burgers-Rott model (Burgers 1948, Rott 1958) can be expressed as (Davies-Jones and Wood 2006)

$$V_\theta = 1.4 V_{\theta z\max} (r/r_{cz})^{-1} \left\{1 - \exp\left[-1.2564 (r/r_{cz})^2\right]\right\}. \qquad (7)$$

The curves representing the Sullivan model follow the expression proposed by Wood and Brown (2011), where

$$V_\theta = V_{\theta z\max} (r/r_{cz})^{2.4} \left[0.3 + 0.7 (r/r_{cz})^{7.89}\right]^{-0.435}, \qquad (8)$$

which is obtained through a numerical fit of the original form derived by Sullivan (1959).

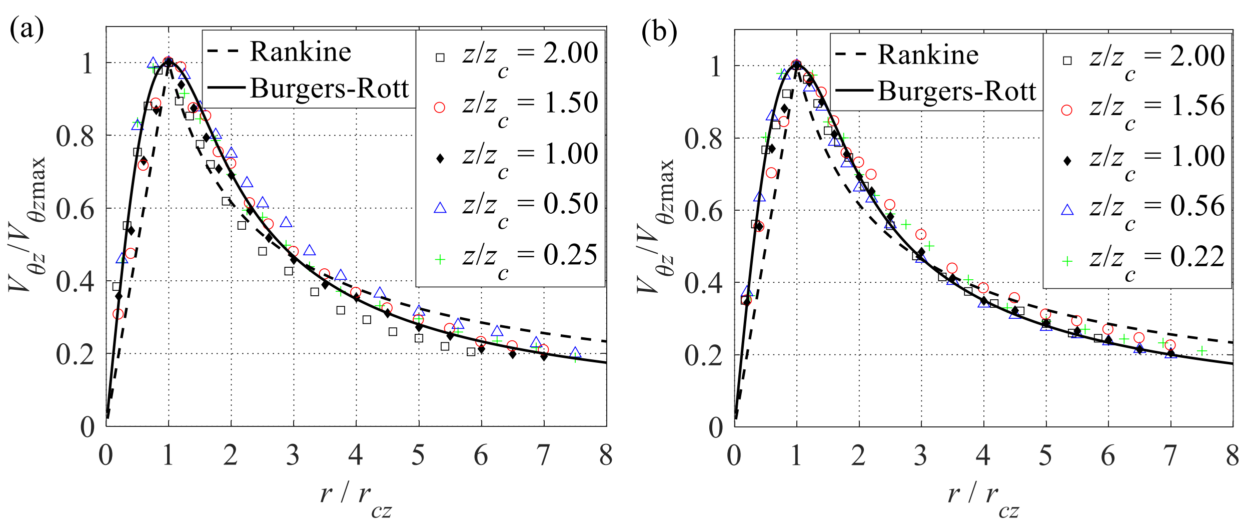

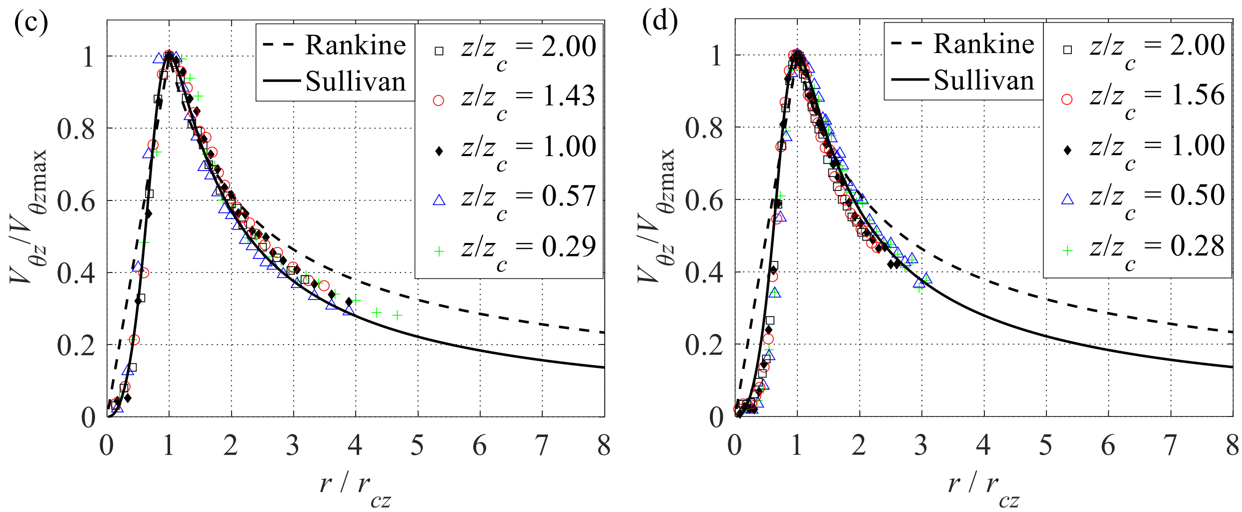


**Fig 4** Radial profiles of mean tangential velocity component at swirl ratios of (a) $S = 0.17$, (b) $S = 0.22$, (c) $S = 0.36$ and (d) $S = 0.84$.

Figure 4 suggests that at all the heights considered, the radial profiles of the mean tangential velocity component of the single-celled vortices agree well with that prescribed by the Burgers-Rott model, and that the corresponding profiles of the dual-celled vortices agree well with that prescribed by the Sullivan model. However, regardless of the number of cells, the profiles of the mean tangential velocity component do not closely follow that prescribed by the Rankine combined-vortex model. The different performances of the three models result from the failure of the Rankine combined-vortex model to consider the radial and axial velocity components, while the Burgers-Rott and Sullivan models consider all three (i.e., tangential, radial and axial) velocity components, and thereby more closely represent the physically simulated vortices. In particular, because the Rankine combined-vortex model essentially treats the flow inside the core of the vortex as a rotating rigid body, it cannot represent the curved profile of the mean tangential velocity component of the flow inside the vortex core.

Figure 5 shows the axial profile of the mean tangential velocity component at the representative core radius $r_c$, and those at a number of locations inside and outside $r_c$, with differences apparent in both cases. At all four swirl ratios, while the axial profiles of the mean tangential velocity component at the positions far outside the representative core radius (e.g., $r \geq 2.6r_c$) resemble the mean velocity profile for straight-line flow above a smooth flat plate, at the positions around or inside the representative core radius, the axial profiles of the mean tangential velocity component become much more complex. For example, inside the representative core radius (i.e., $r \leq r_c$), the mean tangential velocity component increases with height from the floor until reaching a maximum value, presumably partly due to the shear in the boundary layer near the floor, and then decreases until reaching a near-constant value at greater heights. The effect of the swirl ratio is manifested in the rate at which the mean tangential velocity component changes from the edge of the core to the inner part of the core. At a given height, the differences between the mean tangential velocity component at approximately $r/r_c = 0.4$ and $r/r_c = 1$ are relatively minor for the two single-celled vortices at smaller swirl ratios, while for the dual-celled vortices, the differences between the normalized mean tangential velocity component at similar relative locations are much larger.

Figure 6 shows five axial profiles of the mean radial velocity component for each of the four vortices: one at the position of the representative core radius, and two each at positions inside and outside the representative core radius. For all four swirl ratios, the maximum positive (i.e., directed towards the centre of the vortex) mean radial velocity component at the two radial positions outside the representative core radius is found at the very lowest measurement height, which, according to previous studies (e.g., Lewellen and Lewellen 2007), results from the combination of a reduced mean tangential velocity component near the surface (observable in Fig. 5), as well as a strong radial pressure gradient inherited from the larger tangential velocity component of the flow above. For all four swirl ratios, the mean radial velocity component at each radial position outside the representative core radius remains approximately constant at greater heights, coinciding with the mean tangential velocity component at the respective radial positions outside the core radius also being approximately constant over these heights (Fig. 5).

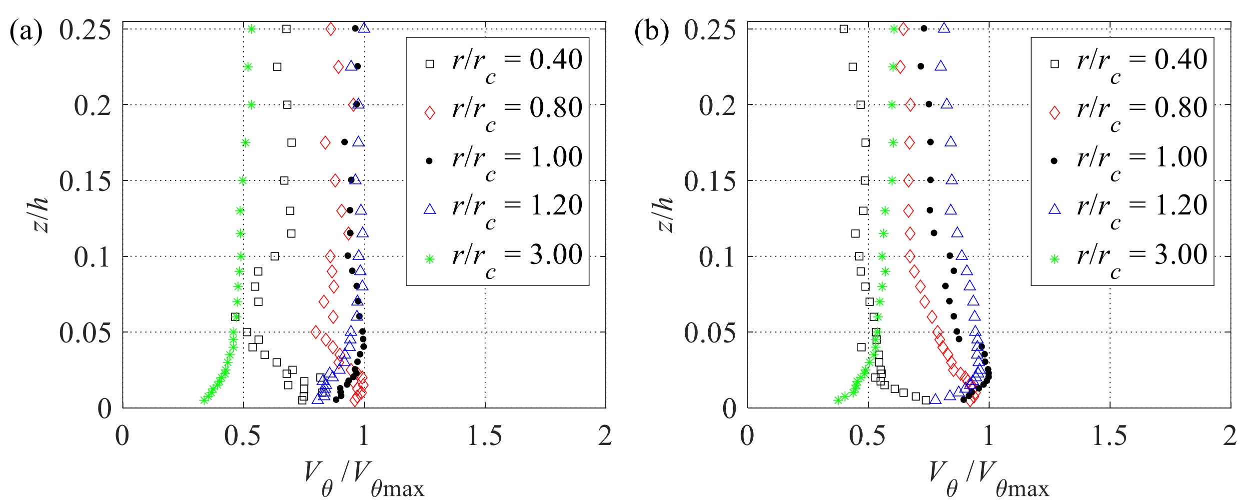

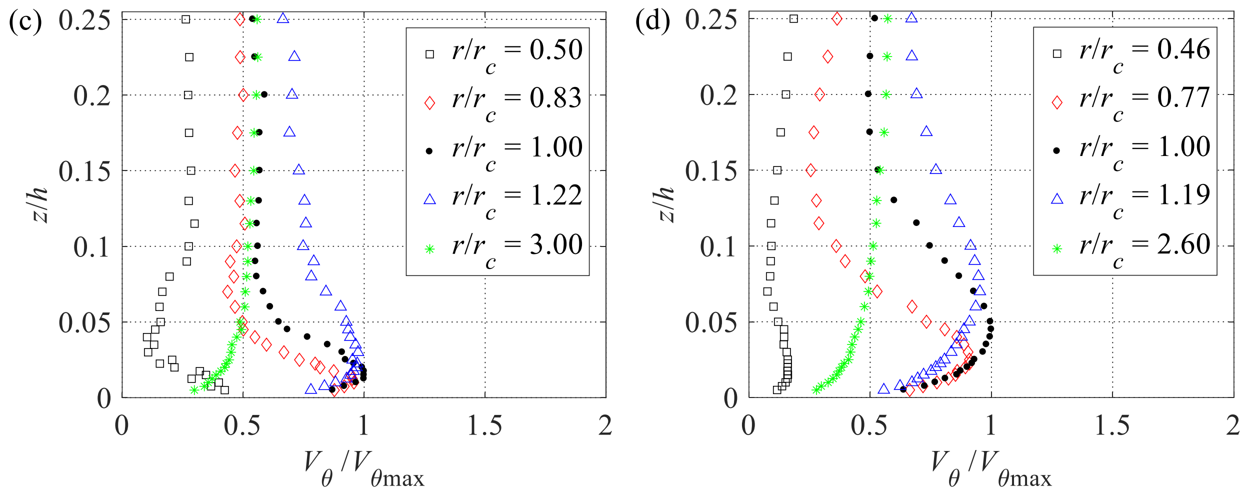


**Fig 5** Axial profiles of the mean tangential velocity component at swirl ratios of (a) $S = 0.17$, (b) $S = 0.22$, (c) $S = 0.36$ and (d) $S = 0.84$.

Inside the core radius, the structure of the mean radial velocity component is much more complex. At the two lower swirl ratios of 0.17 and 0.22, the mean radial velocity component at the very lowest measurement heights inside the representative core radius decreases from maximum positive values until reversing direction and developing into a significant outwards radial velocity component. As seen in Fig. 2, the direction reversal of the mean radial velocity component at these swirl ratios occurs after the flow turns upwards as it converges inwards from the inlet. At the higher swirl ratios of 0.36 and 0.84 after the critical transition, a negative mean radial velocity component also develops at very low elevations. However, as shown in Fig. 2, the negative mean radial velocity component over most of the region inside the representative core radius is a result of the downdraft at the centre of the simulator turning outwards and then back upwards as it approaches the floor.

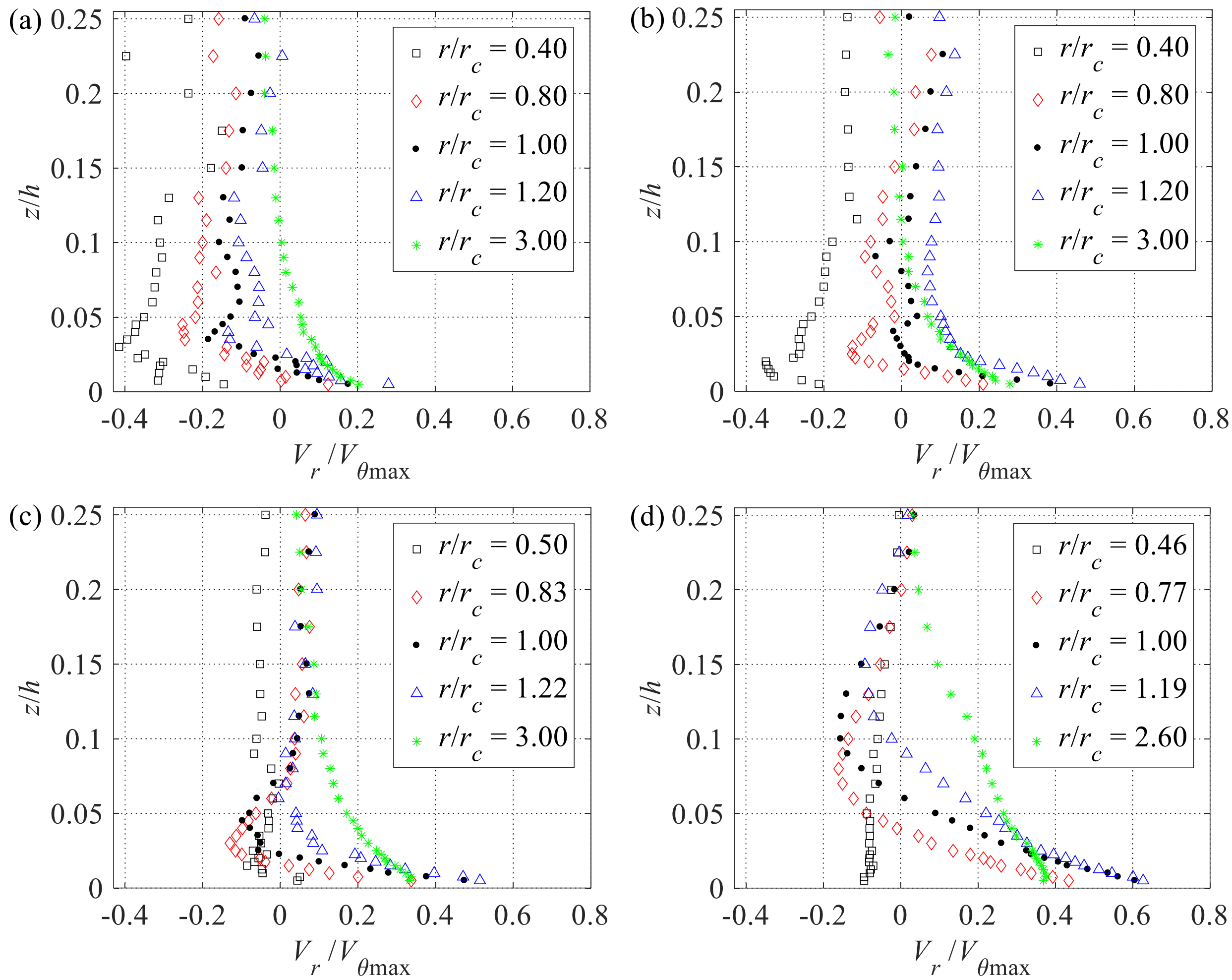


**Fig 6** Axial profiles of the mean radial velocity component at swirl ratios of (a) $S = 0.17$, (b) $S = 0.22$, (c) $S = 0.36$ and (d) $S = 0.84$.

## 5.2 Turbulent velocity components

As noted above, due to the limitation of the Omniprobe in measuring turbulence and that of the Cobra probe in measuring flow directions beyond a 45° cone around the axis of its head, high-frequency measurements of the velocity could only be conducted at positions over restricted regions outside the cores of the vortices. These limited measurements, however, enable an evaluation of the characteristics of the turbulence in regions outside the core. Hence, several characteristics of the fluctuating tangential velocity component are presented for illustrative purposes.

Figure 7 shows contour plots of the turbulence intensity of the tangential velocity component ( $I_{V_\theta} = \sigma_{v_\theta} / V_\theta$, where $\sigma_{v_\theta}$ is the standard deviation of the tangential velocity component) over various regions of the four vortices based on measurements by the Cobra probe. For all four vortices, the fluctuation of the tangential velocity component increases closer to the edges of the cores. However, an apparent difference is observed between the turbulence intensities of the tangential velocity component in the regions close to the core of the two single-celled vortices ( $S = 0.17$ and $S = 0.22$ ) and those in the equivalent regions of the two dual-celled vortices ( $S = 0.36$ and $S = 0.84$ ). For the single-celled vortices, the change of turbulence intensity along the height of the measurement in this region is insignificant, while for the dual-celled vortices, the turbulence intensities at greater heights are much higher than those at lower heights. This is in agreement with an observation made based on Fig. 3 that the local core radii of the two single-celled vortices does not change significantly over the height of measurement, but those of the two dual-celled vortices do.

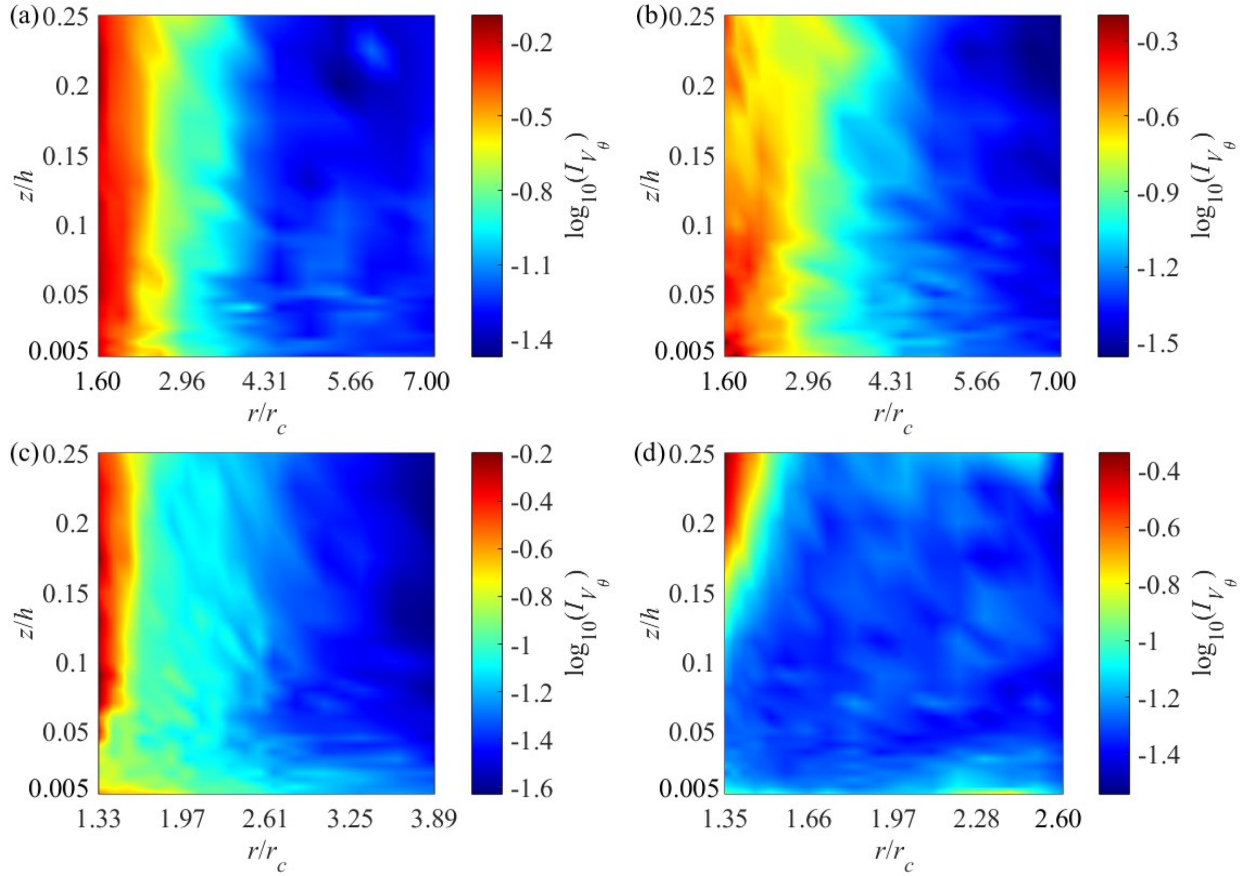


**Fig 7** Turbulence intensity of the tangential velocity component over various regions of the vortices generated at swirl ratios of (a) $S = 0.17$, (b) $S = 0.22$, (c) $S = 0.36$ and (d) $S = 0.84$.

Figure 8 further shows the axial profiles of the turbulence intensity of the tangential velocity component at three discrete radial locations for the four vortices. Over regions far outside the representative core radii of all four vortices, the low turbulence intensity of the tangential velocity component increases with height over lower elevations, but remains practically constant at greater elevations, and thus resembles the vertical profile of the turbulence intensity for straight-line flows over a smooth flat surface. This is consistent with the axial profiles of the mean tangential velocity component at radial positions sufficiently outside the core radius (see Fig. 5) also resembling the vertical profile of the mean wind speed of straight-line flows over a smooth flat surface. At radial positions close to the representative core radii, the axial profiles of the much higher turbulence intensities become complex.

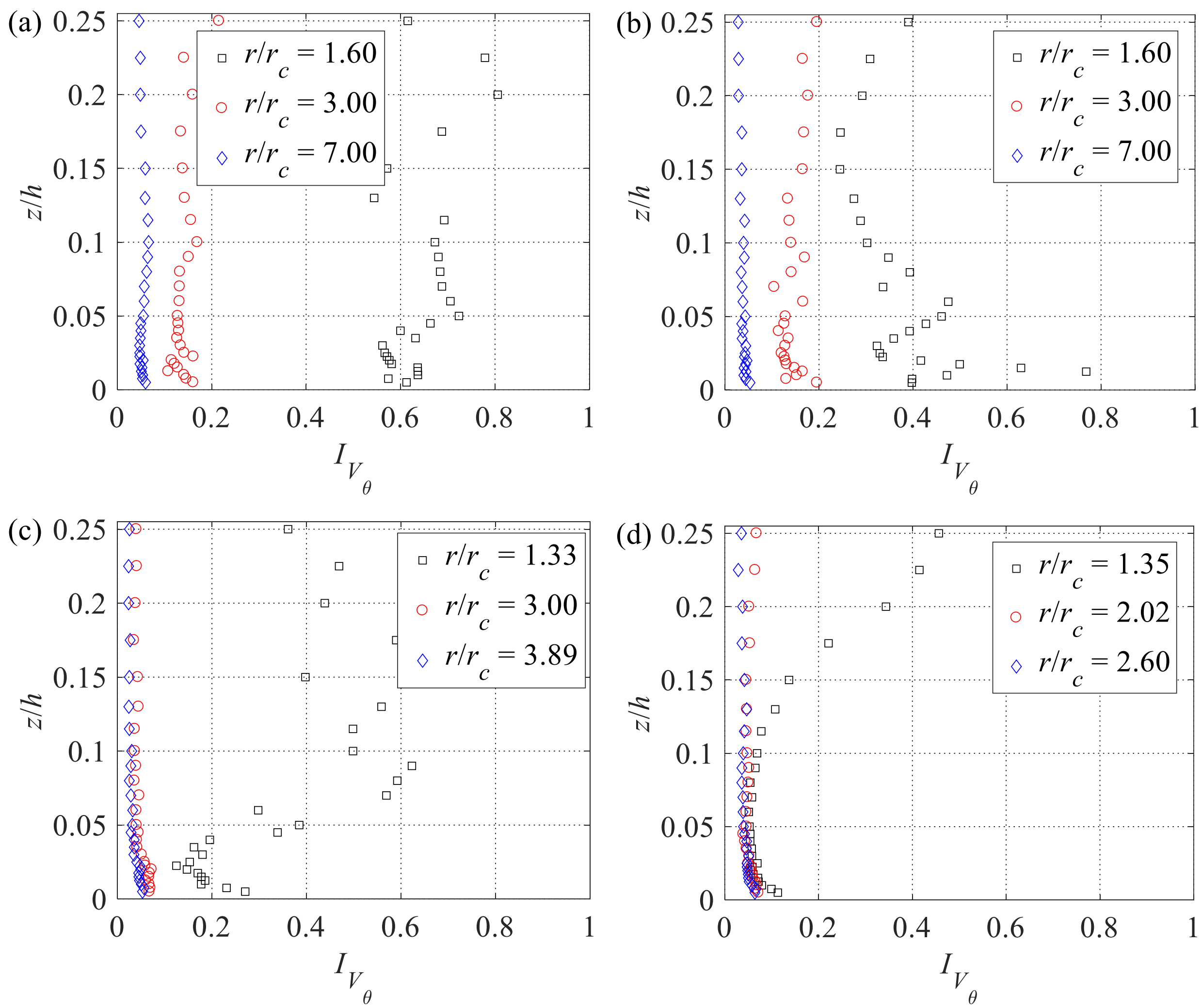


**Fig 8** Axial profiles of turbulence intensity of the tangential velocity component at swirl ratios of (a) $S = 0.17$, (b) $S = 0.22$, (c) $S = 0.36$ and (d) $S = 0.84$.

Figures 9 and 10 show contour plots of the skewness and kurtosis, respectively, of the fluctuating tangential velocity component based on measurements by the Cobra probe. Over the most turbulent regions surrounding the cores of the vortices (see Fig. 7), the skewness can be significantly non-zero and the kurtosis > 3, implying a highly non-Gaussian nature of tangential velocity fluctuations in these regions, with significant implications for the peak tornado loading on structures, as the degree of skewness and kurtosis of the turbulence can significantly influence the probability distribution of the peak loading.

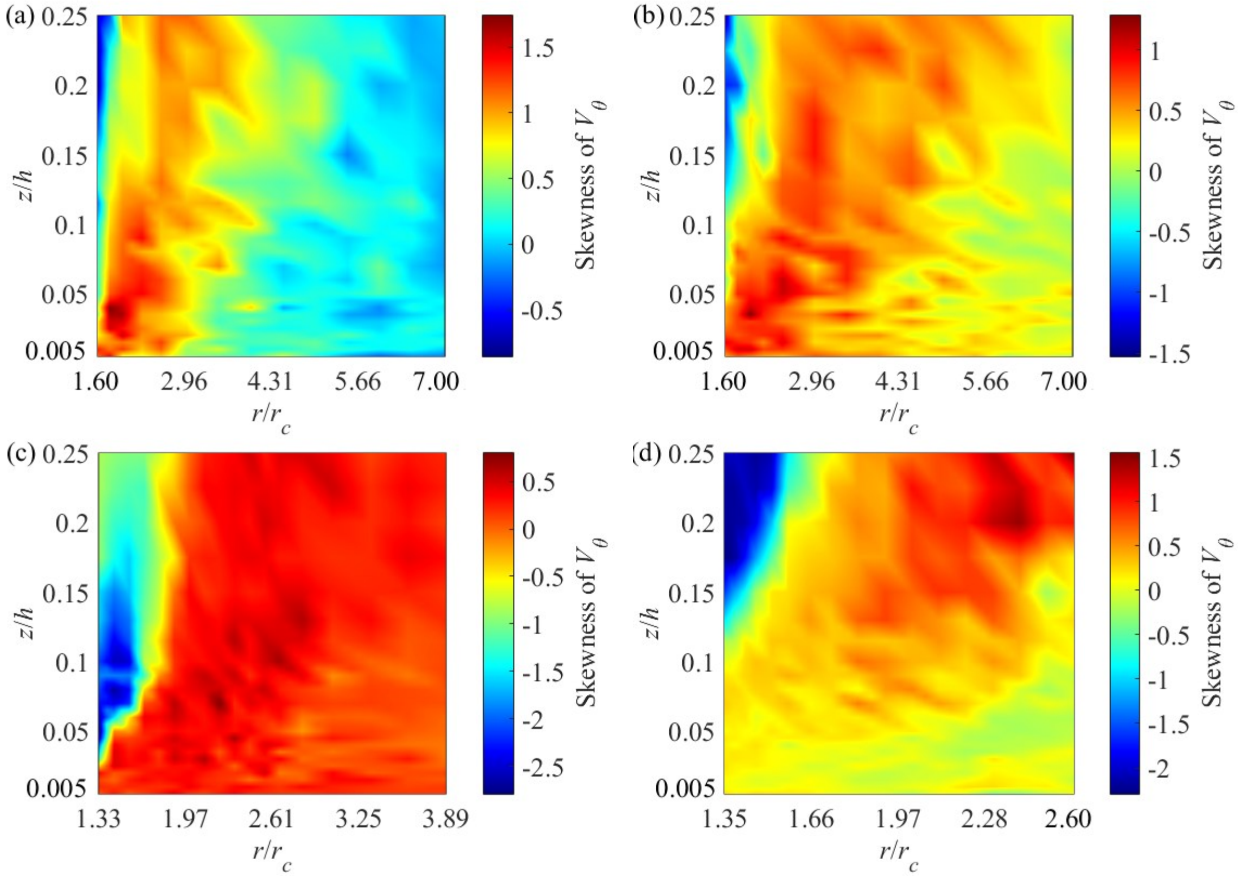


**Fig 9** Skewness of the tangential velocity component over various regions of the vortices generated at swirl ratios of (a) $S = 0.17$, (b) $S = 0.22$, (c) $S = 0.36$ and (d) $S = 0.84$.

Because the high-frequency measurement of the velocity further towards the core of the simulated vortices was not possible, a more comprehensive evaluation of the turbulence, including both the radial and axial components, is not attempted. Instead, the surface-pressure measurements are presented and used as a basis to infer the turbulence characteristics.

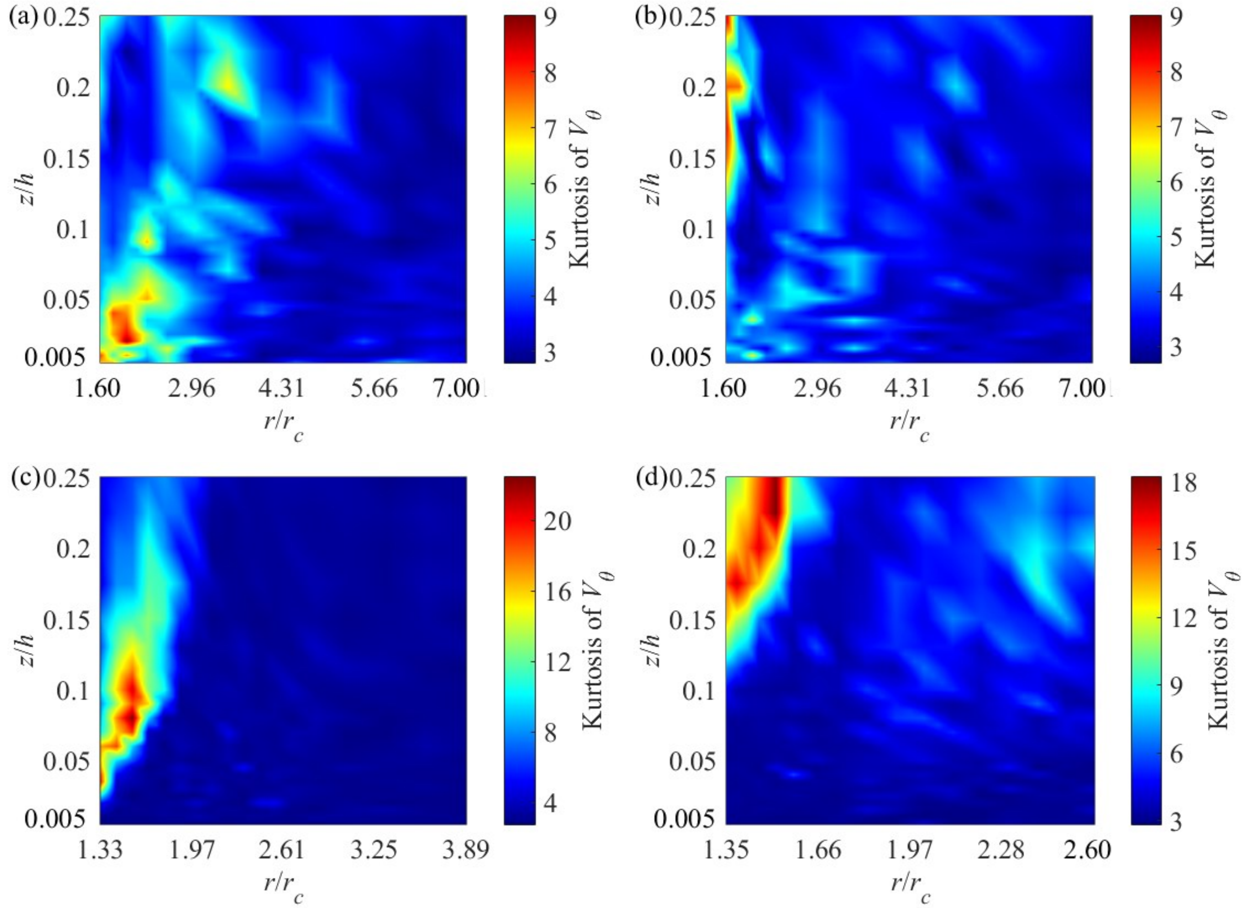


**Fig 10** Kurtosis of the tangential velocity component over various regions of the vortices generated at swirl ratios of (a) $S$ = 0.17, (b) $S$ = 0.22, (c) $S$ = 0.36 and (d) $S$ = 0.84.

## 5.3 Mean surface-pressure deficit

The static-pressure deficit of the air in a tornado can be a significant contributing factor to the overall loading on structures. This is fundamentally different from the loading on structures by straight-line winds where the effect of the static pressure is trivial. Our data suggests that the swirl ratio critically affects not only the mean static-pressure deficit at the surface, which has been revealed by many previous studies (e.g., Snow et al. 1980), but also the fluctuation of the surface pressure. The mean and turbulent characteristics of the surface pressure reflect the characteristics of the flow in the region immediately above the surface, where certain physical structures reside, such as low-rise buildings. To characterize the effect of the swirl ratio on the surface pressure, additional simulations to those for the illustration of the flow were conducted in the VorTECH facility at various swirl ratios, with the radial Reynolds numbers of these additional experiments also between $3.11 \times 10^5$ and $4 \times 10^5$. Figure 11a depicts the radial profiles of the mean surface-pressure deficit ($P$) at the swirl ratios tested, with every value representing the average of 10 mean values as estimated from an ensemble of samples of 2-min duration. The significant level of mean surface-pressure deficit near the centre of the simulated vortices and the transition of the mean surface-pressure-deficit profile due to the corresponding transition of the flow is clearly observed in Fig. 11a. Specifically, the magnitude of the mean surface-pressure deficit around the centre of chamber floor initially increases with increasing swirl ratio, and produces a single sharp pressure drop. As the swirl ratio further increases, the profiles flatten, and eventually develop into a shape with two valleys. A similar evolution of the mean surface-pressure-deficit profile with increasing swirl ratio has been observed in a number of previous studies (e.g., Snow et al. 1980, Refan and Hangan 2016) and attributed to the transition of the flow from a single-celled vortex to a dual-celled vortex with increasing swirl ratio. In particular, according to a previous study (Snow et al. 1980), the rise of the pressure near the centre of the profiles exhibiting two valleys results from the deceleration of the downflow from above the surface in a dual-celled vortex, which agrees with our observations. For example, evident in Fig. 2 for a swirl ratio of 0.84 is a downdraft around the axis of the dual-celled vortex which apparently weakens closer to the surface.

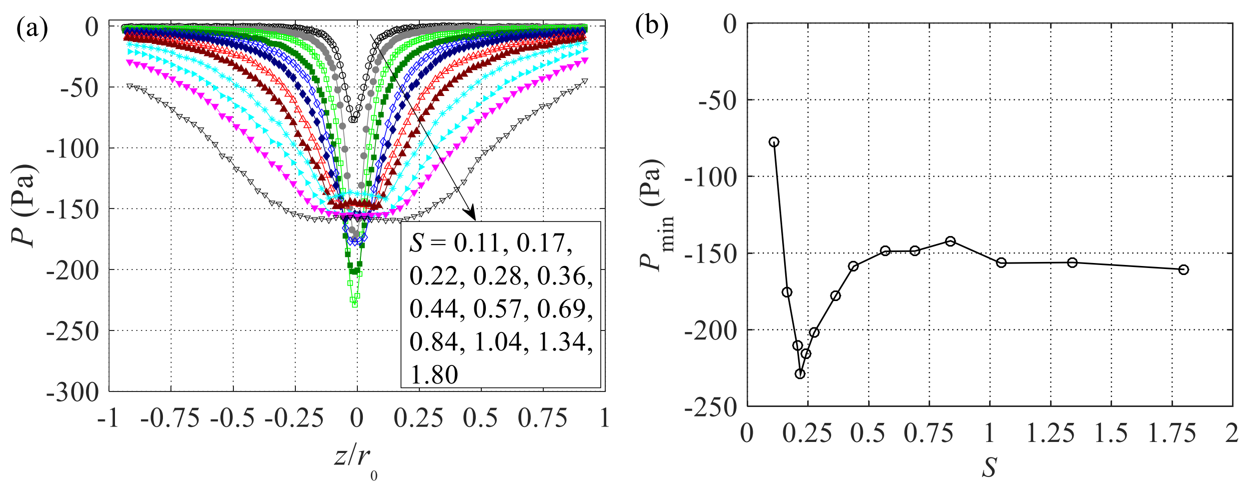


**Fig 11** (a) Profiles of mean surface-pressure deficit and (b) the minimum mean-pressure deficit as a function of the swirl ratio.

Further evidence reflecting the dependence of the mean surface-pressure deficit on the swirl ratio is the largest mean surface-pressure deficit for every profile with the corresponding swirl ratio in Fig. 11b. The minimum value of the mean pressure deficit first decreases and then increases with increasing swirl ratio, with the critical point separating these two regimes corresponding to a swirl ratio of 0.22, which signifies the breakdown of the single-celled vortex extending to the surface. According to previous studies (Church et al. 1979, Refan and Hangan 2016), the transition of the flow from a single-celled-vortex regime to that of a two-celled vortex soon follows with a further increase of the swirl ratio. This observation based on the surface-pressure measurements is also in agreement with observations of the velocity (e.g., Fig. 2), indicating the critical transition occurs between swirl ratios of 0.22 and 0.36.

Comparisons between the flows in prototype tornadoes and tornado-like vortices simulated in laboratories have traditionally been challenging due to the lack of high-fidelity, high-resolution full-scale measurements, especially near the ground. However, high-quality measurements of static pressure at the ground during the passage of tornadoes have become available in recent years, which enable a comparison between the surface-pressure deficits of full-scale tornados with those of simulated tornadoes. Figure 12 shows the mean profiles of the surface-pressure deficit estimated based on measurements in four tornadoes (Karstens et al. 2010) and four corresponding profiles based on our measurements. Normalization of the pressure and radial coordinate is achieved using the absolute value of the maximum mean pressure deficit $|P_{\min}|$, and the radius at which half of the maximum mean pressure deficit is reached $r_{0.5p_{\min}}$, respectively. The resemblances between the normalized full-scale and laboratory profiles are apparent. According to Karstens et al. (2010), the two Manchester tornadoes are single-celled in structure, the Tipton tornado has a dual-celled structure, but it is unclear whether the Webb tornado is of a single-celled or dual-celled structure, which is remarkably consistent with our conclusions, as the transition between single-celled and dual-celled vortices occurs at a swirl ratio between 0.22 and 0.36. Indeed, that it is challenging to discern whether the Webb tornado is single-celled or dual-celled results from the swirl ratio being close to the critical transition.

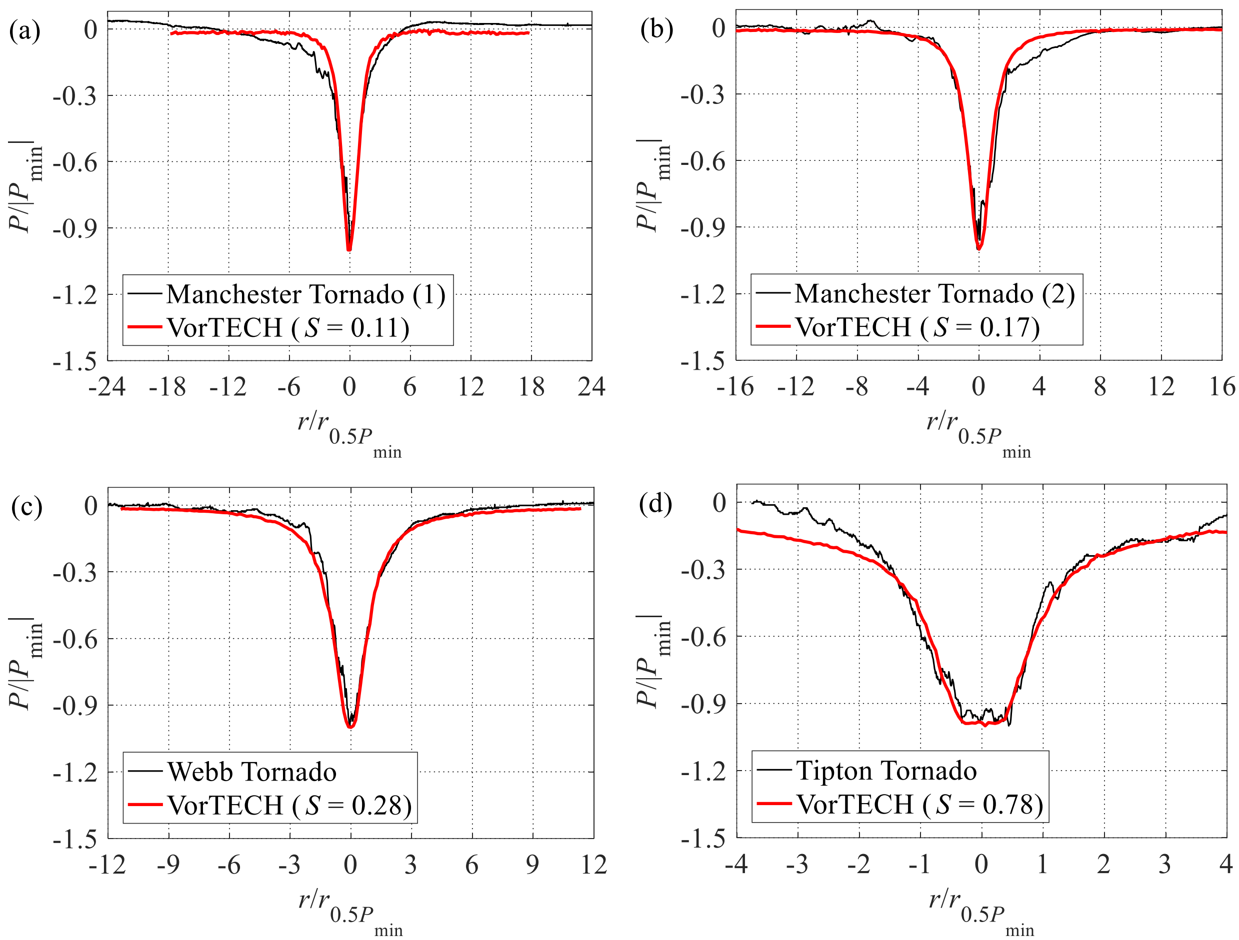


**Fig 12** Comparison between radial profiles of mean surface-pressure deficit of full-scale and simulated tornado vortices.

## 5.4 Fluctuating surface-pressure deficit

The pressure measurements suggest that the swirl ratio also critically affects the fluctuation of the surface-pressure deficit. Figure 13 shows the radial profiles of the first four moments of the surface-pressure deficit for the four representative vortices analysed above. The mean value of the surface-pressure deficit shown in Fig. 11a is presented here as the mean pressure coefficient defined as $C_P = P/(0.5\rho V_{\theta\max}^2)$, where $\rho$ is the air density, and the second moment is represented by the variance of the pressure normalized by the absolute value of the maximum pressure deficit. Each value represents the ensemble average of the corresponding statistics based on the 10 individual test runs. While the effect of the swirl ratio on the mean pressure deficit is again apparent, the dependence of the fluctuations of the pressure on the swirl ratio is also clearly observed in Fig. 13. According to the profile of the normalized variance, the surface pressure fluctuates significantly over the regions inside and immediately surrounding the cores of the four vortices, and the most significant fluctuations occur inside the cores. When the vortex transitions from a single-celled structure at small swirl ratios to a dual-celled structure at higher swirl ratios, the radial distribution of the variance of the surface-pressure deficit transitions from a bell-shaped profile to symmetric bi-modal shaped, suggesting the effects of the swirl ratio on the pressure fluctuation.

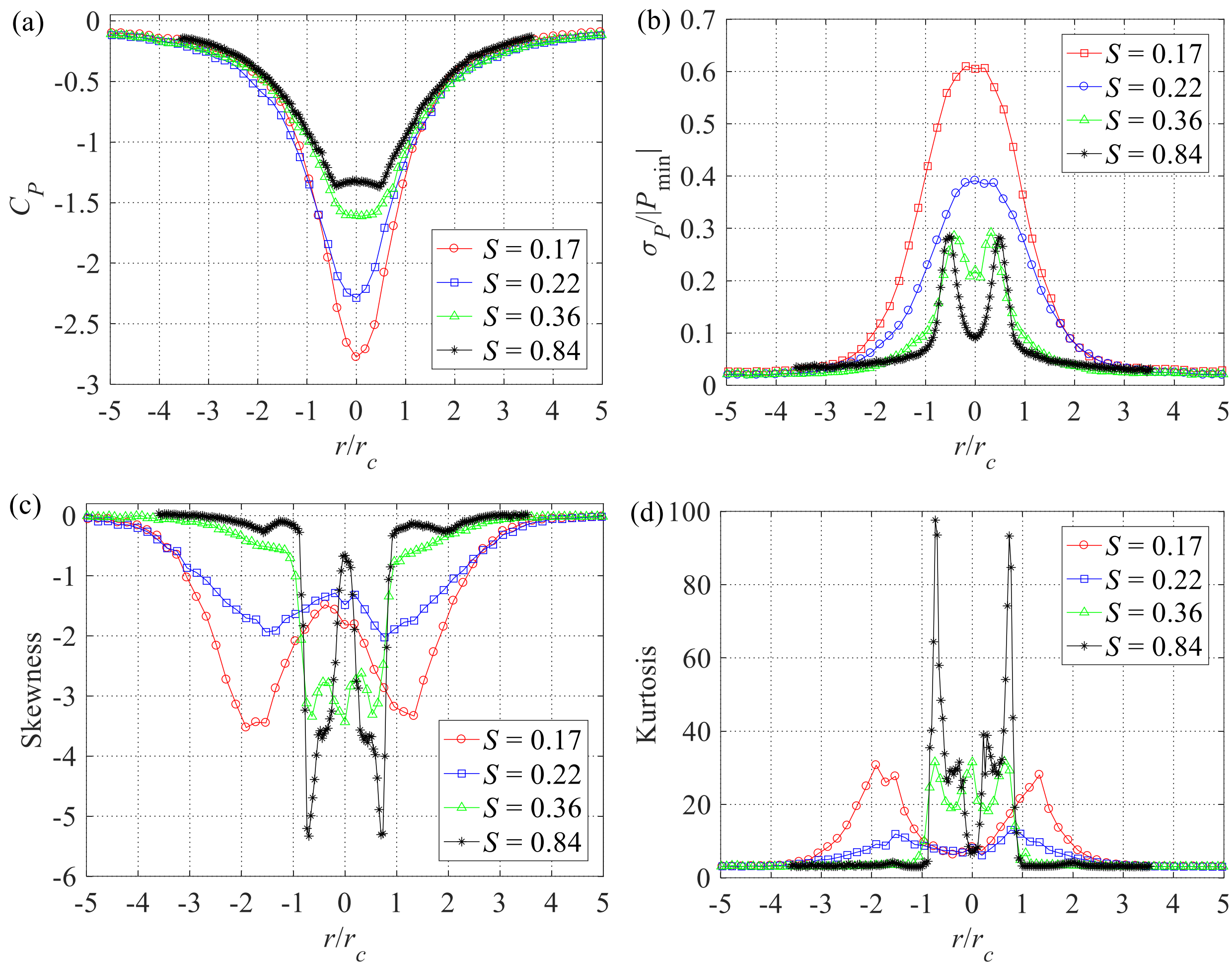


**Fig 13** Dependence of surface pressure on swirl ratio for the (a) mean pressure coefficient (b) standard deviation, (c) skewness and (d) kurtosis of the pressure fluctuations.

In addition, the skewness and kurtosis profiles shown in Fig. 13 suggest that while the surface-pressure fluctuation over regions far outside the representative core radius of each vortex exhibits Gaussian characteristics (i.e., the skewness and the kurtosis are around zero and 3, respectively), the pressure fluctuation over the regions in and immediately surrounding the core radii of all four vortices are highly non-Gaussian. Further, Fig. 13 clearly reveals the effect of the swirl ratio on the 3rd and 4th moments of the pressure fluctuation. While the profiles of the skewness and kurtosis of the surface pressure beneath the two single-celled vortices (i.e., $S = 0.17$ and $S = 0.22$) are essentially symmetric and bi-modal in shape, the profiles of the skewness and kurtosis of the surface pressure beneath the two dual-celled vortices ($S = 0.36$ and $S = 0.84$) are also essentially symmetric, but much more complex in shape. Moreover, for the two single-celled vortices, the higher the swirl ratio, the more the skewness and kurtosis of the pressure fluctuation deviate from the corresponding values for Gaussian processes. However, the manner in which the skewness and kurtosis of the pressure fluctuation at a specific radial position depends on the swirl ratio is much more complex for the dual-celled vortices.

Although a comprehensive evaluation of the correlation between the characteristics of the flow and those of the surface-pressure fluctuations is not possible due to the incompleteness of the velocity measurements, the surface-pressure fluctuation is undoubtedly a result of the turbulence immediately aloft. Indeed, some characteristics of the turbulence over the regions of the flow with high-frequency velocity measurements are observed to be qualitatively well correlated with some corresponding characteristics of the surface-pressure fluctuation. For example, a comparison between Figs. 13 and 7 suggests that, in the case of the two single-celled vortices, significant fluctuations of the tangential velocity and surface pressure are present at radial positions between two and three times the respective representative core radii, and become progressively much more intense at radial positions towards the axis of the simulator. Also, by comparing Fig. 13 with Figs. 9 and 10, it can be seen that over the radial positions where the fluctuation of the surface pressure beneath the two single-celled vortices is significantly non-Gaussian, the fluctuation of the flow over the regions immediately above these radial positions also exhibits significant non-Gaussian characteristics. In the case of the two dual-celled vortices, however, the correlations between the characteristics of the surface pressure and those of the flow aloft cannot be clearly identified even in a qualitative manner. This is because, as shown in Figs. 7 and 13, significant fluctuations of the surface pressure or the flow immediately above the surface do not occur at the radial positions over which high-frequency velocity measurements are made. Nevertheless, it is reasonable to infer based on the observed characteristics of the surface-pressure fluctuation that, for both single-celled and dual-celled vortices, the fluctuation of the near-surface flow over certain ranges of radial position can be highly non-Gaussian, which can significantly influences the probability distribution of the loading on structures by tornadoes.

## 6 Effects of radial Reynolds number

While the characteristics of the simulated flow and the those of the surface-pressure deficit both clearly depend on the swirl ratio, previous studies have shown that simulation of a tornado-like vortex does not depend critically on the radial Reynolds number, provided this number is sufficiently large (e.g., Church et al. 1979, Refan and Hangan 2016). However, previous studies have primarily focused on the effects of the radial Reynolds number on the mean components of the flow and surface pressure. Here, the flow field of two vortices simulated at distinct radial Reynolds numbers and the mean and fluctuating surface pressure beneath vortices for various radial Reynolds numbers help illustrate that neither the mean nor the fluctuating velocity and surface pressure depend on the radial Reynolds number, as long as this parameter is sufficiently large.

Figure 14a, b depicts the mean flow field of two vortices simulated at different radial Reynolds numbers of $3.91 \times 10^5$ and $3.02 \times 10^5$, respectively, but with practically identical swirl ratios ($S$ = 0.44). The structures of the mean flow fields are similar despite the differences in the magnitudes of the respective velocity components. Figure 14c, d presents the axial profiles of the normalized local core radius and the normalized maximum mean tangential velocity component of the two vortices, where despite substantial differences in the radial Reynolds number, the profiles are practically identical corresponding to the identical swirl ratios.

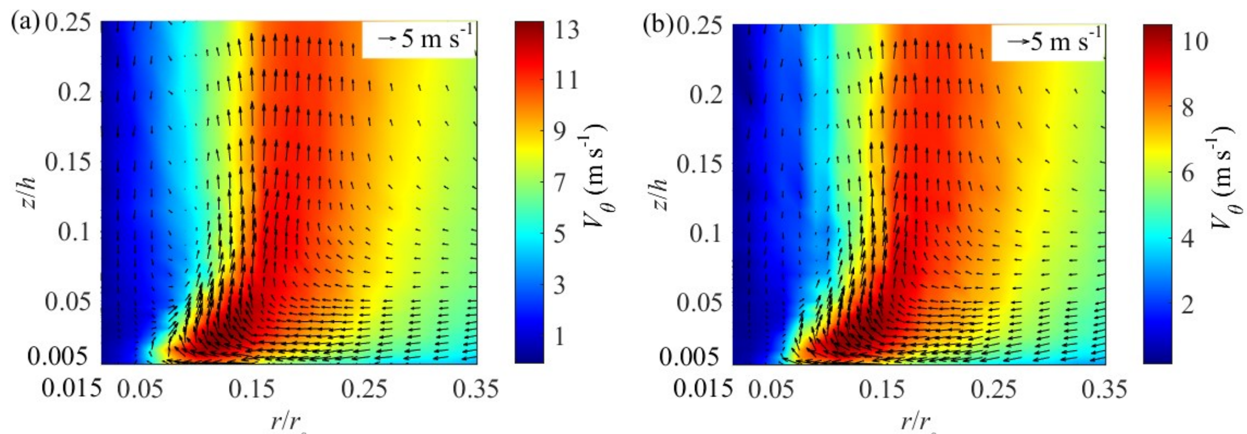

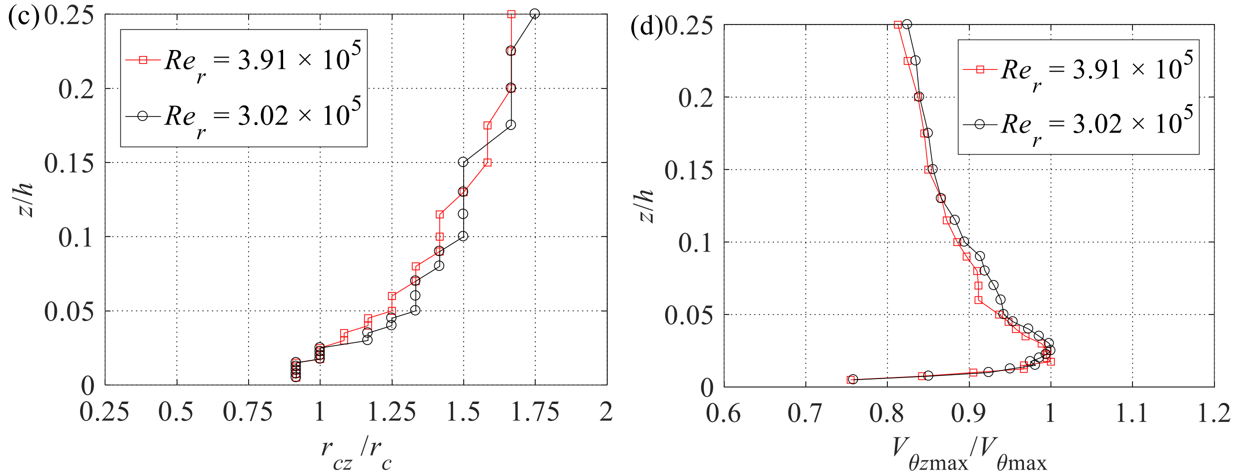


**Fig 14** Mean flow fields of vortices simulated at radial Reynolds numbers of (a) $Re_r = 3.91 \times 10^5$ and (b) $Re_r = 3.02 \times 10^5$, and profiles of (c) local core radius and (d) maximum mean tangential velocity component at these two radial Reynolds numbers.

Figure 15 shows profiles of the normalized mean value and standard deviation, as well as the skewness and kurtosis of the surface-pressure deficit beneath vortices for three radial Reynolds numbers. The radial Reynolds number apparently does not significantly affect the mean or fluctuating surface pressure over the regions where these two components are significant. However, while significant effects of the radial Reynolds number on the 2nd to 4th moments of the pressure fluctuation at radial positions far from the cores of the vortices are present, this is because the surface-pressure deficit is very low at these positions for low radial Reynolds numbers and, consequently, the pressure transducers record very weak and thus unreliable signals.

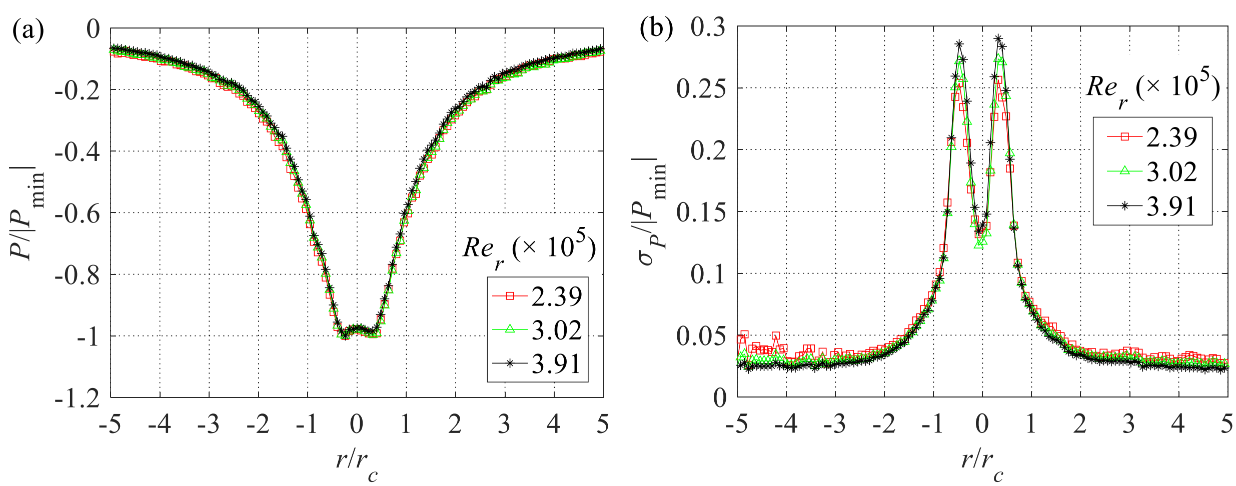

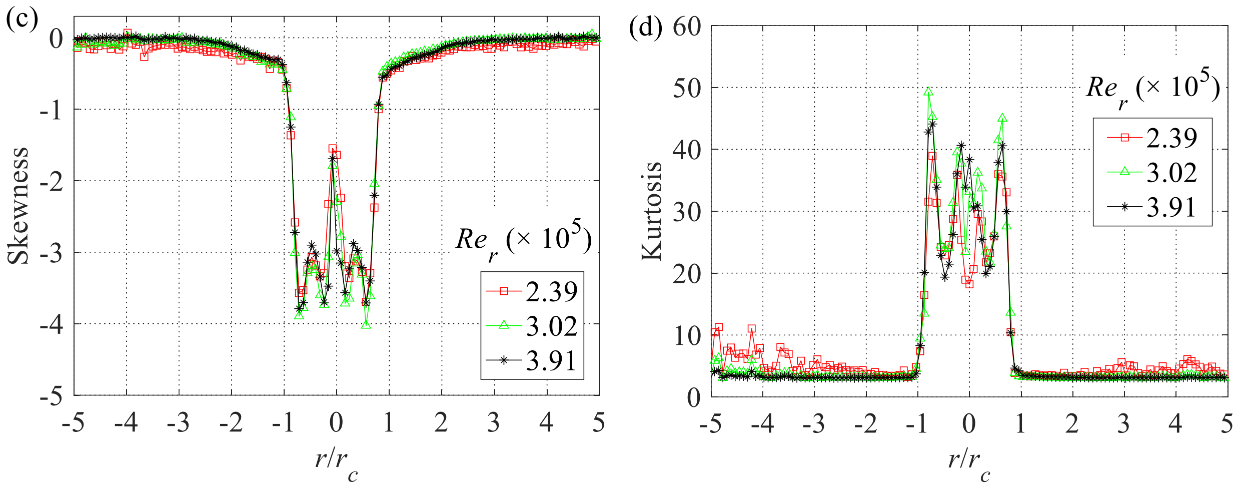


**Fig 15** Dependence of (a) mean, (b) standard deviation, (c) skewness and (d) kurtosis of the surface-pressure deficit on the radial Reynolds number.

## 7 Conclusions and discussions

Tornado-like vortices are generated in a large-scale Ward-type tornado simulator to investigate the mean and fluctuating characteristics of tornado-like flows and their dependence on the swirl ratio and the radial Reynolds number. Measurements of the velocity and surface pressures reveal the significance of the swirl ratio. In particular, the flow transitions from a single-celled to a dual-celled vortex with increasing swirl ratio, with corresponding development of a downdraft in the centre of the vortex following the extension of vortex breakdown to the surface. This transition results in the single-celled and dual-celled vortices exhibiting distinct mean and turbulent flow structures, as well as a corresponding transition of the mean and fluctuating surface-pressure deficit. The characteristics of the surface pressure beneath a number of simulated vortices and their dependence on the swirl ratio closely resemble those observed in full-scale tornadoes, which validates the capability of the simulator to generate tornado-like vortices.

The velocity and surface-pressure measurements at various radial Reynolds numbers, and essentially identical swirl ratios, further confirm the important conclusion of previous studies that the laboratory simulation of tornado-like vortices in simulators such as the VorTECH facility is independent of the radial Reynolds number, as long as this number is sufficiently large. It is particularly revealed that the characteristics of the mean and fluctuating velocity and surface pressure are independent of the radial Reynolds number.

While a number of the observations made based on the mean characteristics of the flow and the surface pressure are consistent with previous experiments, the characteristics of the turbulence and surface-pressure fluctuation observed in the experiments have significant implications for the dynamics of simulated tornado-like vortices, as well as the tornado loading on structures. The velocity measurements suggest that the fluctuations of the flow inside and around the tornado core can be highly non-Gaussian, which is different from the case of straight-line winds, for which the turbulence can often be reasonably assumed to be Gaussian. This difference between the turbulence in tornadic and straight-line boundary-layer-type winds can be a source of significant difference between the fluctuating loadings on structures by these two types of flows. Further, the pressure measurements suggest that a large static-pressure deficit develops inside and around the core of a tornado, and that the fluctuation of the pressure deficit in these regions is also highly non-Gaussian. Such characteristics of the static-pressure deficit can also significantly contribute to the tornado loading on structures.

**Acknowledgements** The authors wish to thank Professor William Gallus in the Department of Geological and Atmospheric Sciences at Iowa State University for providing the full-scale surface-pressure measurement data used for comparison with our surface measurements. The authors also want to pay tribute to the late Timothy Samaras, who contributed to the recording of the full-scale surface-pressure data. We acknowledge partial support from the National Science Foundation under award number CMMI 1663363.

## References

Burgers JM (1948) A mathematical model illustrating the theory of turbulence. Adv Appl Mech 1:171–199

Church CR, Snow JT, Agee EM (1977) Tornado Vortex Simulation at Purdue University. Bull Am Meteorol Soc 58(9):900–908

Church C, Snow JT, Baker GL, Agee EM (1979) Characteristics of Tornado-Like Vortices as a Function of Swirl Ratio: A Laboratory Investigation. J Atmos Sci 36(9):1755–1776

Davies-Jones RP (1973) The Dependence of Core Radius on Swirl Ratio in a Tornado Simulator. J Atmos Sci 30(7):1427–1430

Davies-Jones RP, Wood VT (2006) Simulated Doppler velocity signatures of evolving tornado-like vortices. J Atmos Ocean Technol 23(8):1029–1048

Dessens J, Jr. (1972) Influence of Ground Roughness on Tornadoes: A Laboratory Simulation. J Appl Meteorol 11(1):72–75

Haan FL, Sarkar PP, Gallus WA (2008) Design, construction and performance of a large tornado simulator for wind engineering applications. Eng Struct 30(4):1146–1159

Ishihara T, Oh S, Tokuyama Y (2011) Numerical study on flow fields of tornado-like vortices using the LES turbulence model. J Wind Eng Ind Aerodyn 99(4):239–248

Jischke MC, Parang M (1974) Properties of Simulated Tornado-Like Vortices. J Atmos Sci 31(2):506–512

Karstens CD, Samaras TM, Lee BD, Gallus Jr WA, Finley CA (2010) Near-Ground Pressure and Wind Measurements in Tornadoes*. Mon Weather Rev 138(7):2570–2588

Lewellen DC, Lewellen WS (2007) Near-Surface Intensification of Tornado Vortices. J Atmos Sci 64(7):2176–2194

Lewellen WS (1962) A solution for three-dimensional vortex flows with strong circulation. J Fluid Mech 14(03):420–432

Lewellen WS, Lewellen DC, Sykes RI (1997) Large-Eddy Simulation of a Tornado's Interaction with the Surface. J Atmos Sci 54(5):581–605

Liu Z, Ishihara T (2015) Numerical study of turbulent flow fields and the similarity of tornado vortices using large-eddy simulations. J Wind Eng Ind Aerodyn 145:42–60

Lund DE, Snow JT (1993) Laser Doppler Velocimeter Measurements in Tornadolike Vortices, The Tornado: Its Structure, Dynamics, Prediction, and Hazards. American Geophysical Union, Washington, D. C., pp 297–306

Matsui M, Tamura Y (2009) Influence of incident flow conditions on generation of tornado-like flow. In: Proceedings of the 11th Americas Conference on Wind Engineering, Puerto Rico

Mishra AR, James DL, Letchford CW (2008) Physical simulation of a single-celled tornado-like vortex, Part A: Flow field characterization. J Wind Eng Ind Aerodyn 96(8-9):1243–1257

Natarajan D, Hangan H (2012) Large eddy simulations of translation and surface roughness effects on tornado-like vortices. J Wind Eng Ind Aerodyn 104–106:577–584

Nolan DS  (2005) A New Scaling for Tornado-Like Vortices. J Atmos Sci 62(7):2639–2645

Nolan DS, Farrell BF (1999) The Structure and Dynamics of Tornado-Like Vortices. J Atmos Sci 56(16):2908–2936

Refan M, Hangan H (2016) Characterization of tornado-like flow fields in a new model scale wind testing chamber. J Wind Eng Ind Aerodyn 151:107–121

Refan M, Hangan H, Siddiqui K (2015) Physical modelling of tornado-like flow field. In: ASME-JSME-KSME 2015 Joint Fluids Engineering Conference, Seoul, Korea

Refan M, Hangan H, Wurman J (2014) Reproducing tornadoes in laboratory using proper scaling. J Wind Eng Ind Aerodyn 135:136–148

Rott N  (1958) On the viscous core of a line vortex. Z Angew Math Phys 9(5-6):543–553

Snow JT, Church CR, Barnhart BJ (1980) An Investigation of the Surface Pressure Fields beneath Simulated Tornado Cyclones. J Atmos Sci 37(5):1013–1026

Sullivan RD  (1959) A Two-Cell Vortex Solution of the Navier-Stokes Equations. J Aerosp Sci 26(11):767–768

Tari PH, Gurka R, Hangan H (2010) Experimental investigation of tornado-like vortex dynamics with swirl ratio: The mean and turbulent flow fields. J Wind Eng Ind Aerodyn 98(12):936–944

Wang J, Cao S, Pang W, Cao J (2017) Experimental Study on Effects of Ground Roughness on Flow Characteristics of Tornado-Like Vortices. Boundary-Layer Meteorol 162(2):319–339

Wang J, Cao S, Pang W, Cao J, Zhao L (2016) Wind-load characteristics of a cooling tower exposed to a translating tornado-like vortex. J Wind Eng Ind Aerodyn 158:26–36

Ward NB (1972) The Exploration of Certain Features of Tornado Dynamics Using a Laboratory Model. J Atmos Sci 29(6):1194–1204

Wood VT, Brown RA (2011) Simulated Tornadic Vortex Signatures of Tornado-Like Vortices Having One- and Two-Celled Structures. J Appl Meteorol Climatol 50(11):2338–2342

Wurman J, Alexander CR (2005) The 30 May 1998 Spencer, South Dakota, Storm. Part II: Comparison of Observed Damage and Radar-Derived Winds in the Tornadoes. Mon Weather Rev 133(1):97–119

Wurman J, Robinson P, Alexander C, Richardson Y (2007) Low-Level Winds in Tornadoes and Potential Catastrophic Tornado Impacts in Urban Areas. Bull Am Meteorol Soc 88(1):31–46

Ying SJ, Chang CC (1970) Exploratory Model Study of Tornado-Like Vortex Dynamics. J Atmos Sci 27(1):3–14

Zhang W, Sarkar PP (2008) Effects on ground roughness on tornado like vortex using PIV. In: Proceedings of the AAWE workshop, Vail, CO